Supporting information for:

All-conjugated Cationic copolythiophene "rod-rod" block copolyelectrolytes: synthesis, optical properties and solvent dependent assembly

Amandine Thomas,[ab] Judith E. Houston,[c] Niko Van den Brande,[d] Julien De Winter,[e] Michèle Chevrier,[af] Richard K. Heenan,[g] Ann E. Terry,[g] Sébastien Richeter,[a] Ahmad Mehdi,[a] Bruno Van Mele,[d] Philippe Dubois,[e] Roberto Lazzaroni,[b] Pascal Gerbaux,[e] Rachel C. Evans*[ch] and Sébastien Clément*[a]

[a] *Institut Charles Gerhardt – UMR 5253, Equipe Chimie Moléculaire et Organisation du Solide, Université Montpellier 2 – CC1701, Place Eugène Bataillon, F-34095 Montpellier Cedex 05, France. E-mail: sebastien.clement02@univ-montp2.fr; Tel: +33467143971.*
[b] *Laboratory for Chemistry of Novel Materials, Center for Innovation in Materials and Polymers, Research Institute for Science and Engineering of Materials, University of Mons – UMONS, 23 Place du Parc, B-7000 Mons, Belgium.*
[c] *School of Chemistry, The University of Dublin, Trinity College, Dublin 2, Ireland. E-mail: raevans@tcd.ie*
[d] *Physical Chemistry and Polymer Science (FYSC), Vrije Universiteit Brussel (VUB), Pleinlaan 2, B-1050 Brussels, Belgium.*
[e] *Laboratory of organic synthesis and mass spectrometry, Interdisciplinary Centre for Mass Spectrometry, University of Mons-UMONS, 23 Place du Parc, B-7000 Mons, Belgium*
[f] *Laboratory for Polymeric and Composites Materials, Center for Innovation in Materials and Polymers, Research Institute for Science and Engineering of Materials, University of Mons – UMONS, 23 Place du Parc, B-7000 Mons, Belgium.*
[g] *ISIS-CCLRC, Rutherford Appleton Laboratory, Chilton, Oxon OX11 0QX, United Kingdom.*
[h] *Centre for Research on Adaptive Nanostructures and Nanodevices (CRANN), Trinity College Dublin, Dublin 2, Ireland.*

Table of contents:

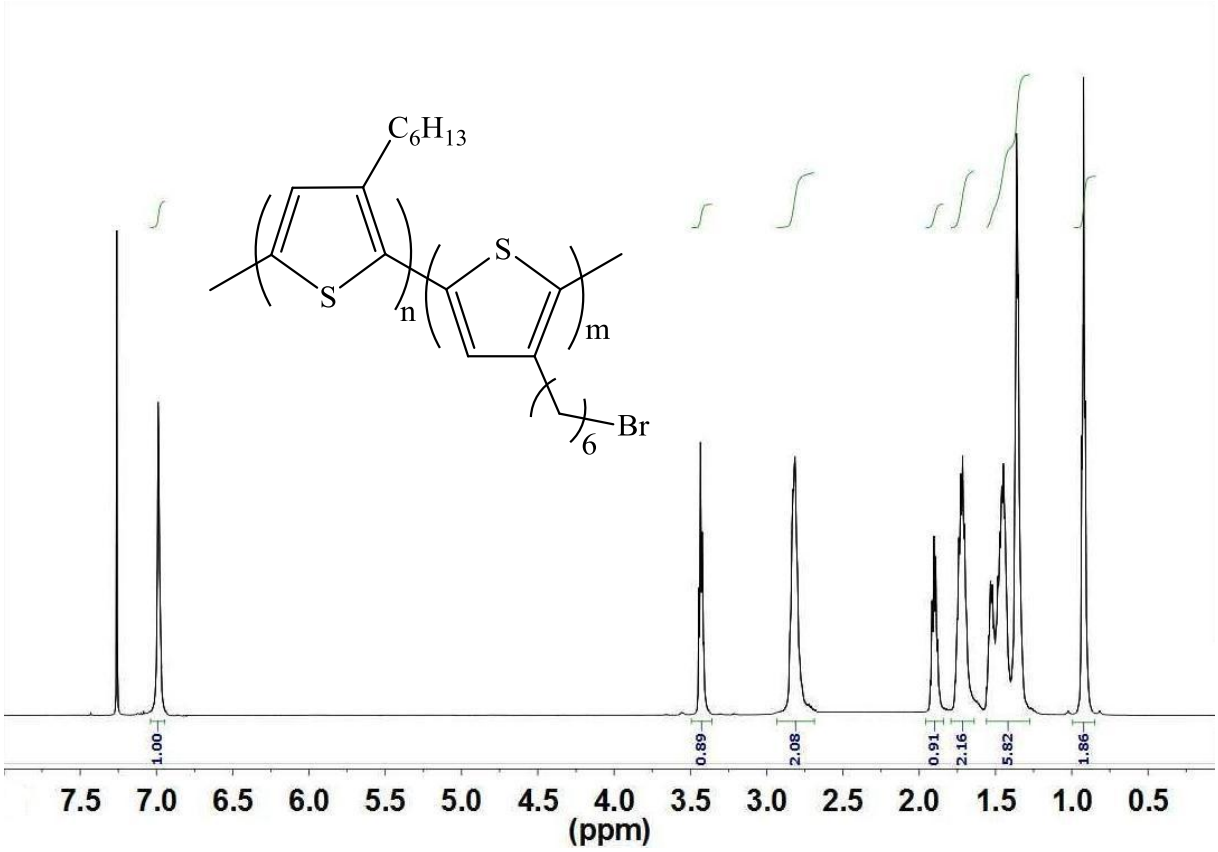

Figure S1. ^{1}H NMR spectrum of **P3HT-*b*-P3HTBr** in $CDCl_3$

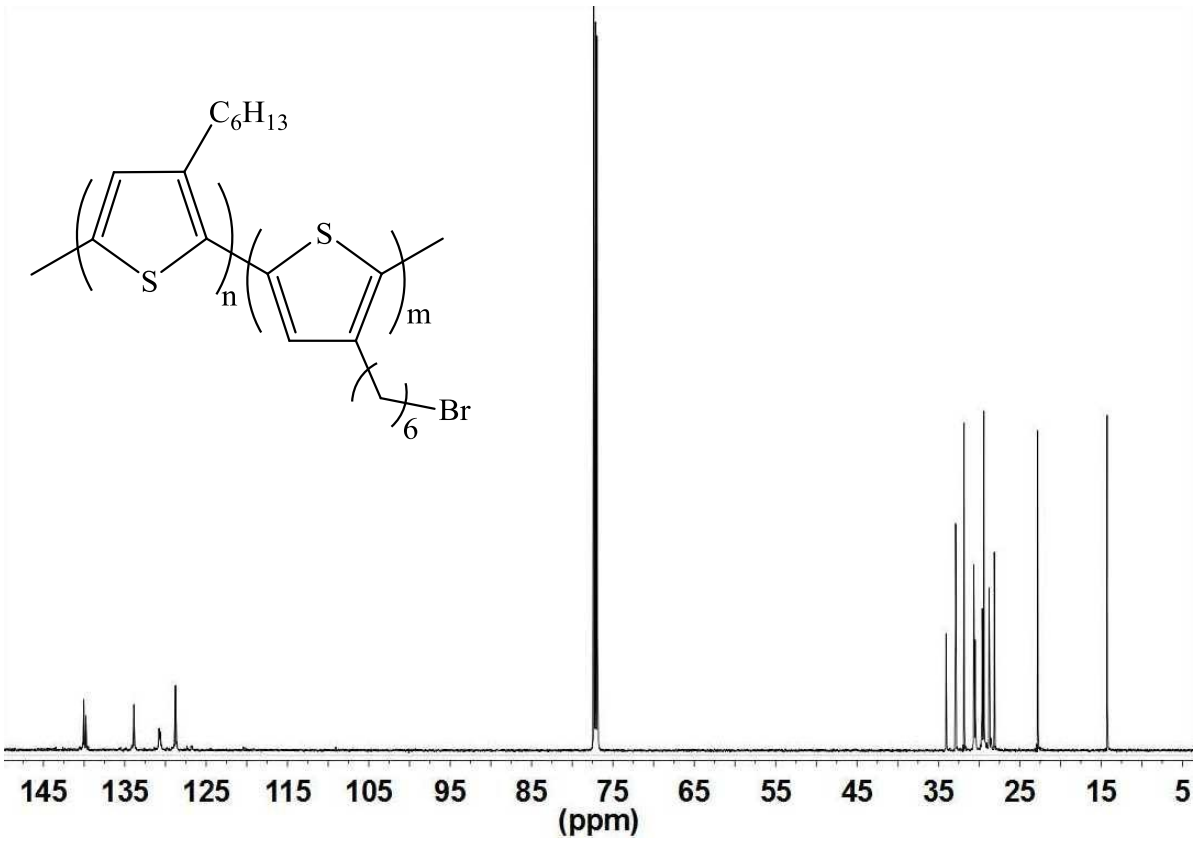

Figure S2. $^{13}C\{^{1}H\}$ NMR spectrum of **P3HT-*b*-P3HTBr** in $CDCl_3$

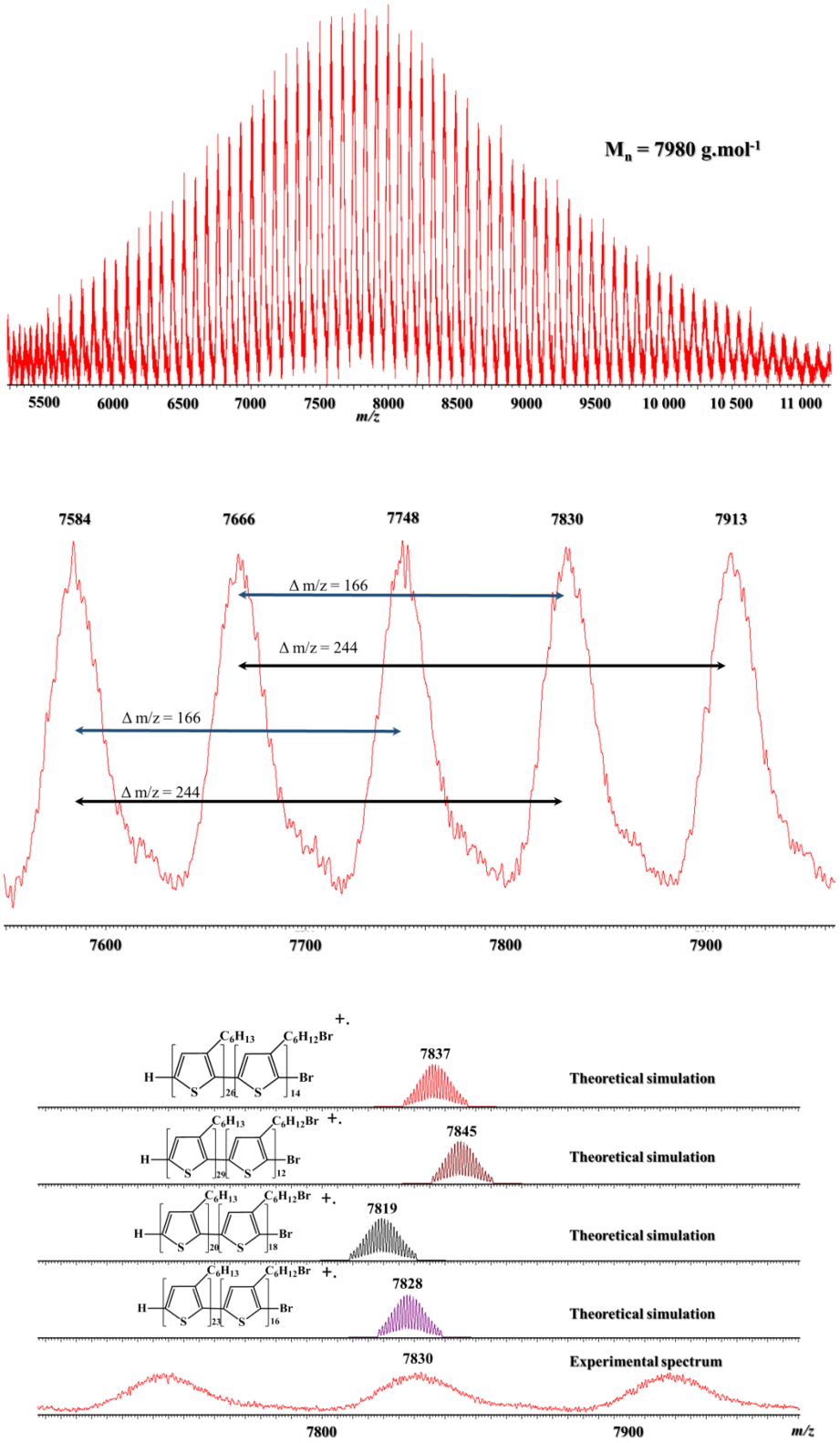

Figure S3. (1) Global MALDI-ToF mass spectrum recorded for **P3HT-b-P3HTBr**, (2) Magnification between *m/z* 7550 and *m/z* 7960. Each signal of the distribution corresponds of an association of many different congeners having close *m/z*, (3) some of them are presented for the signal centred at *m/z* 7830.

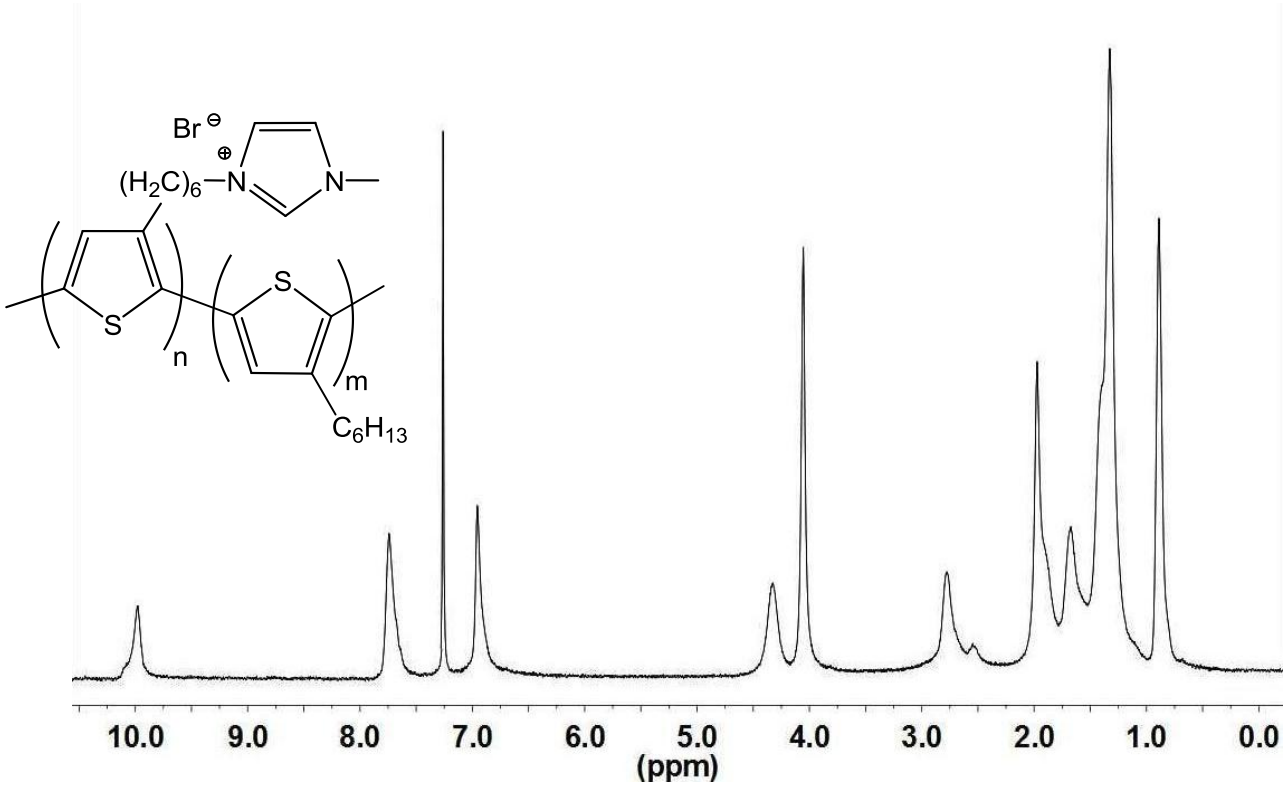

Figure S4. ^{1}H NMR spectrum of **P3HT-*b*-P3HTIm** in $CDCl_3$

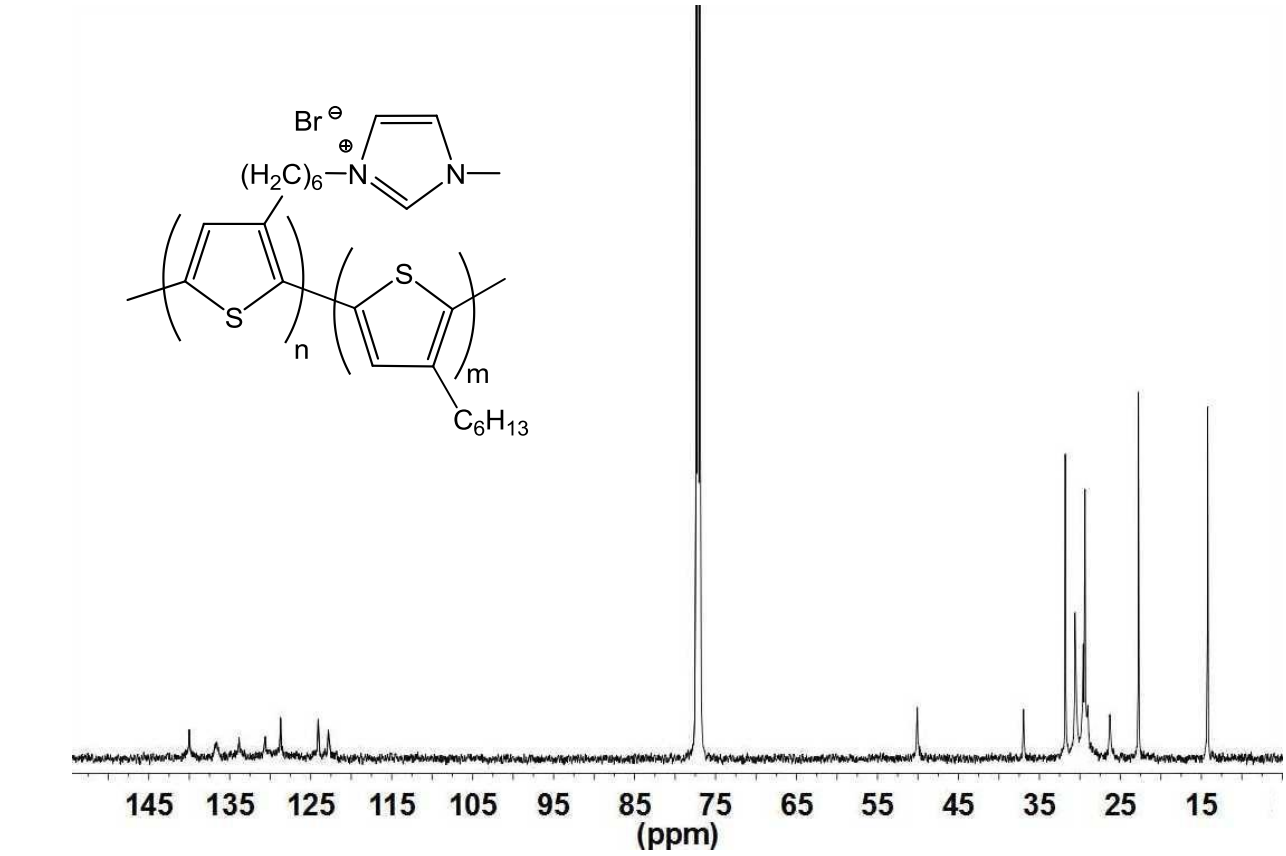

Figure S5. $^{13}C\{^{1}H\}$ NMR spectrum of **P3HT-*b*-P3HTIm** in $CDCl_3$

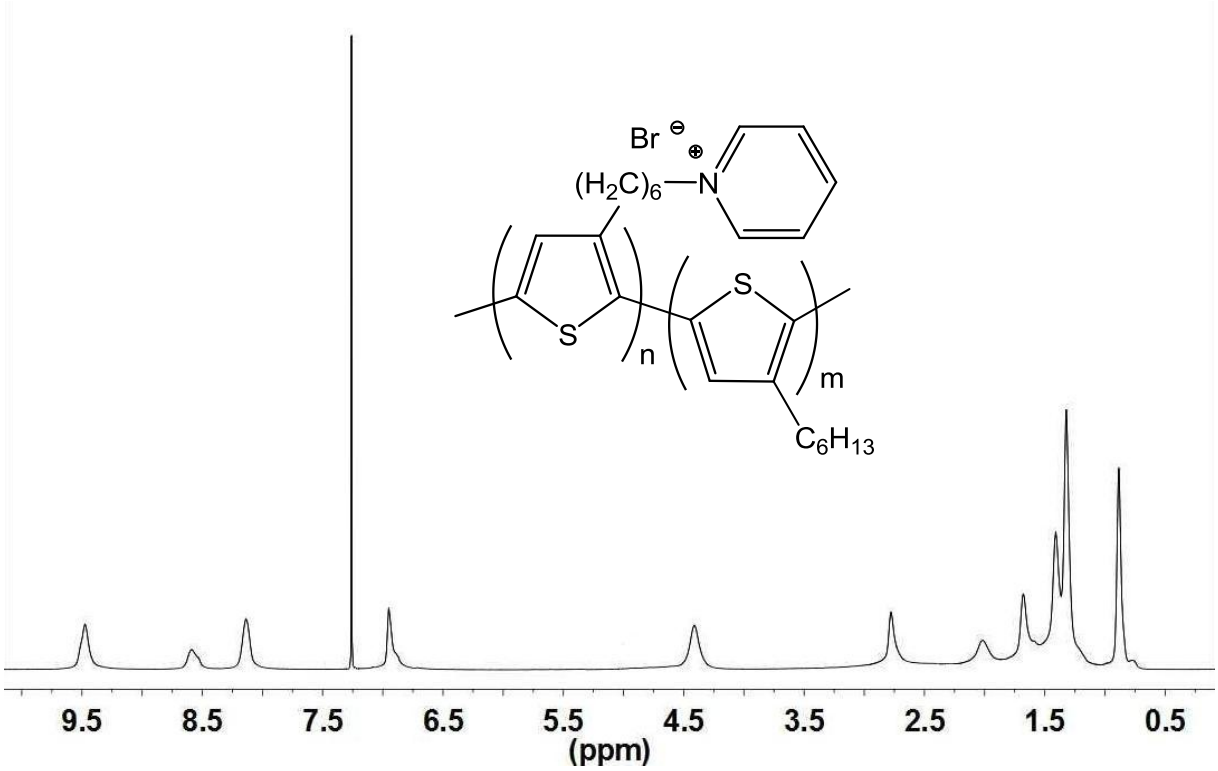

Figure S6. ^{1}H NMR spectrum of **P3HT-*b*-P3HTPy** in $CDCl_3$

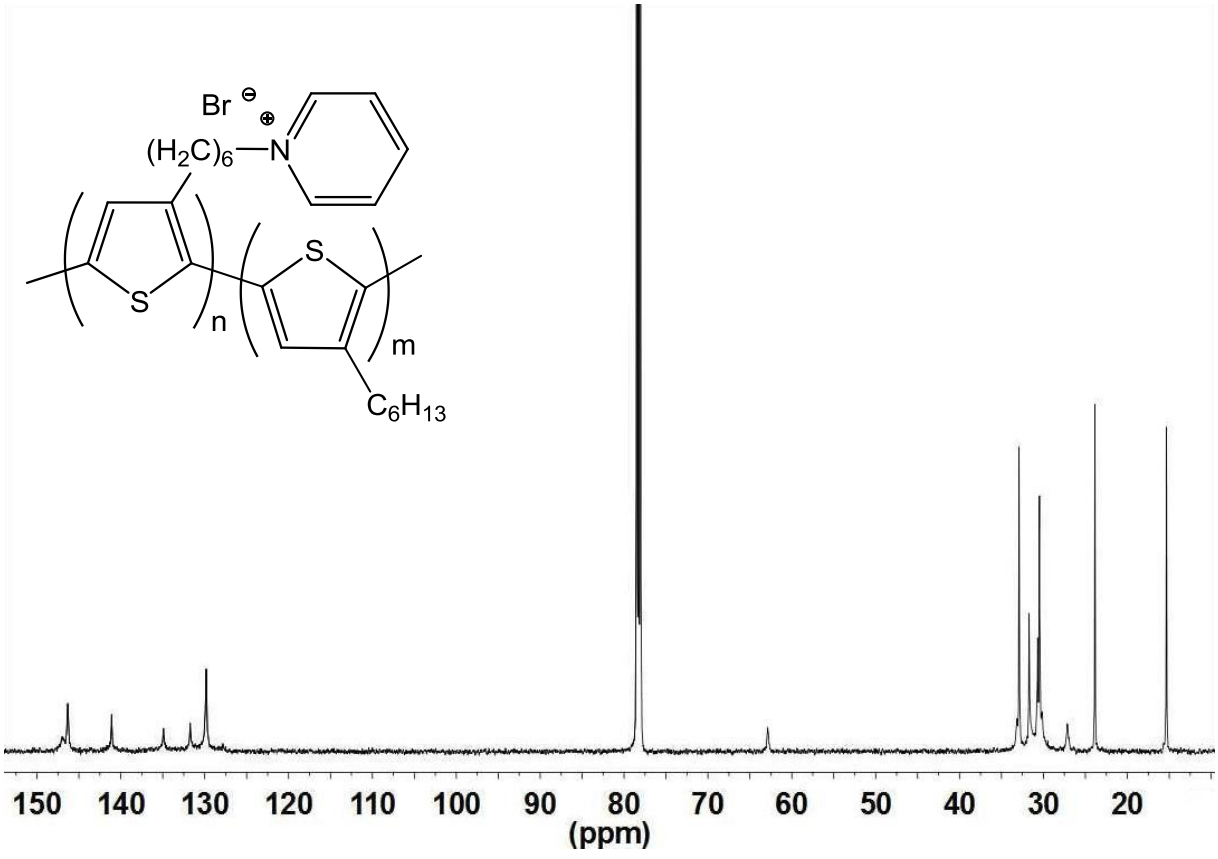

Figure S7. $^{13}C\{^{1}H\}$ NMR spectrum of **P3HT-*b*-P3HTPy** in $CDCl_3$

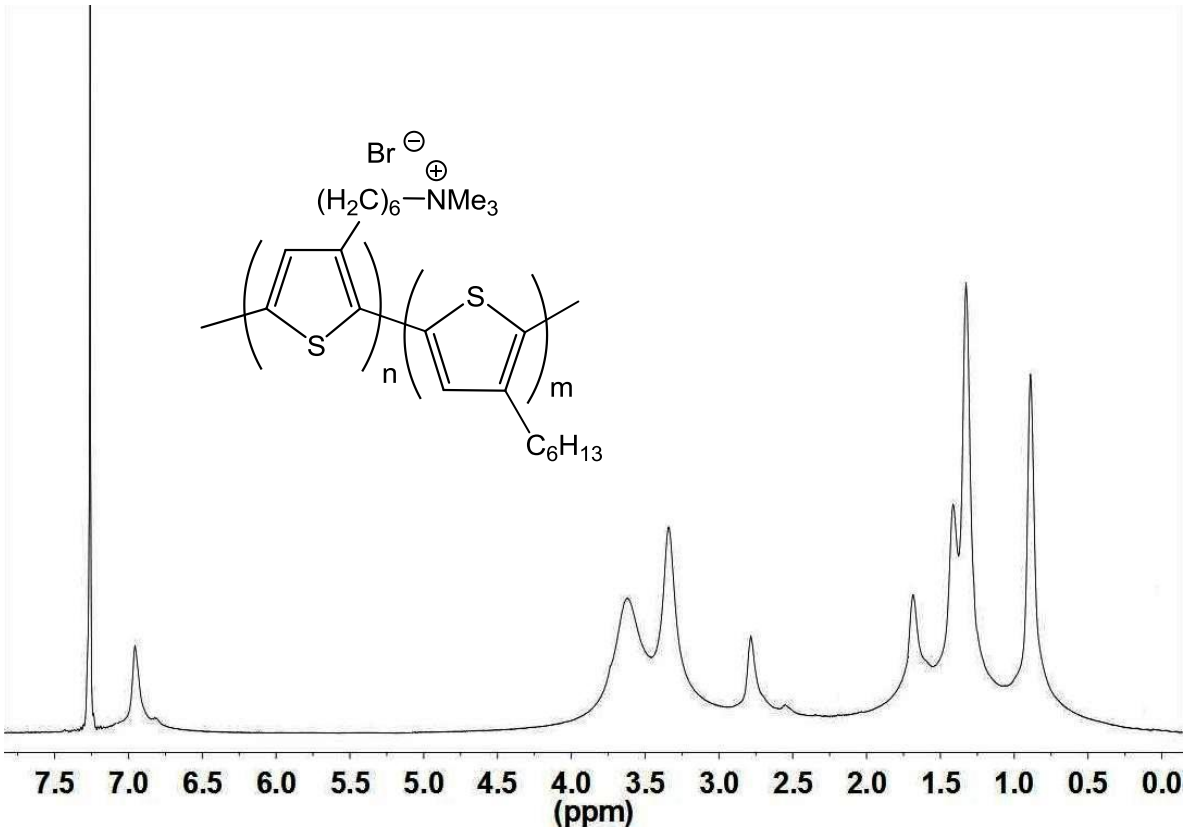

Figure S8. ^{1}H NMR spectrum of **P3HT-*b*-P3HTNMe$_3$** in $CDCl_3$

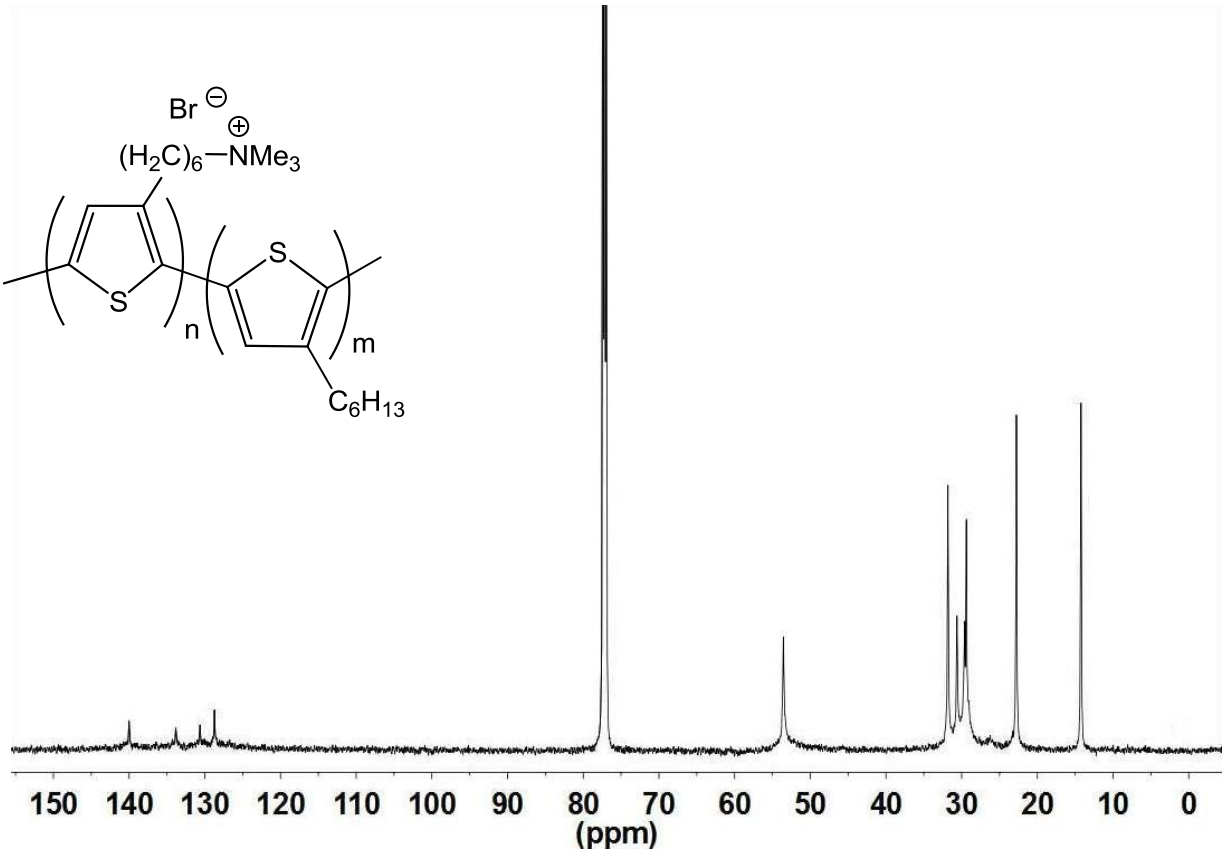

Figure S9. ^{13}C{^{1}H} NMR spectrum of **P3HT-*b*-P3HTNMe$_3$** in $CDCl_3$

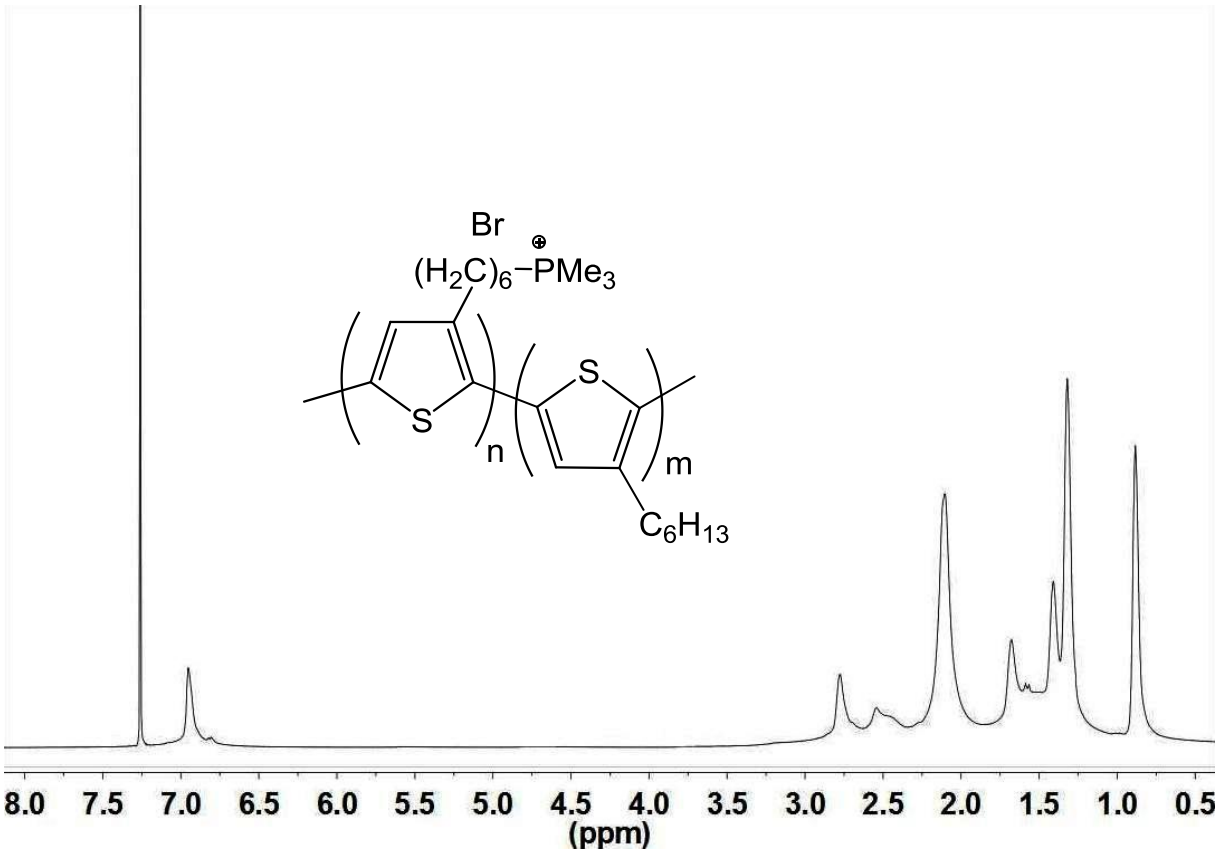

Figure S10. ^{1}H NMR spectrum of **P3HT-*b*-P3HTPMe$_3$** in $CDCl_3$

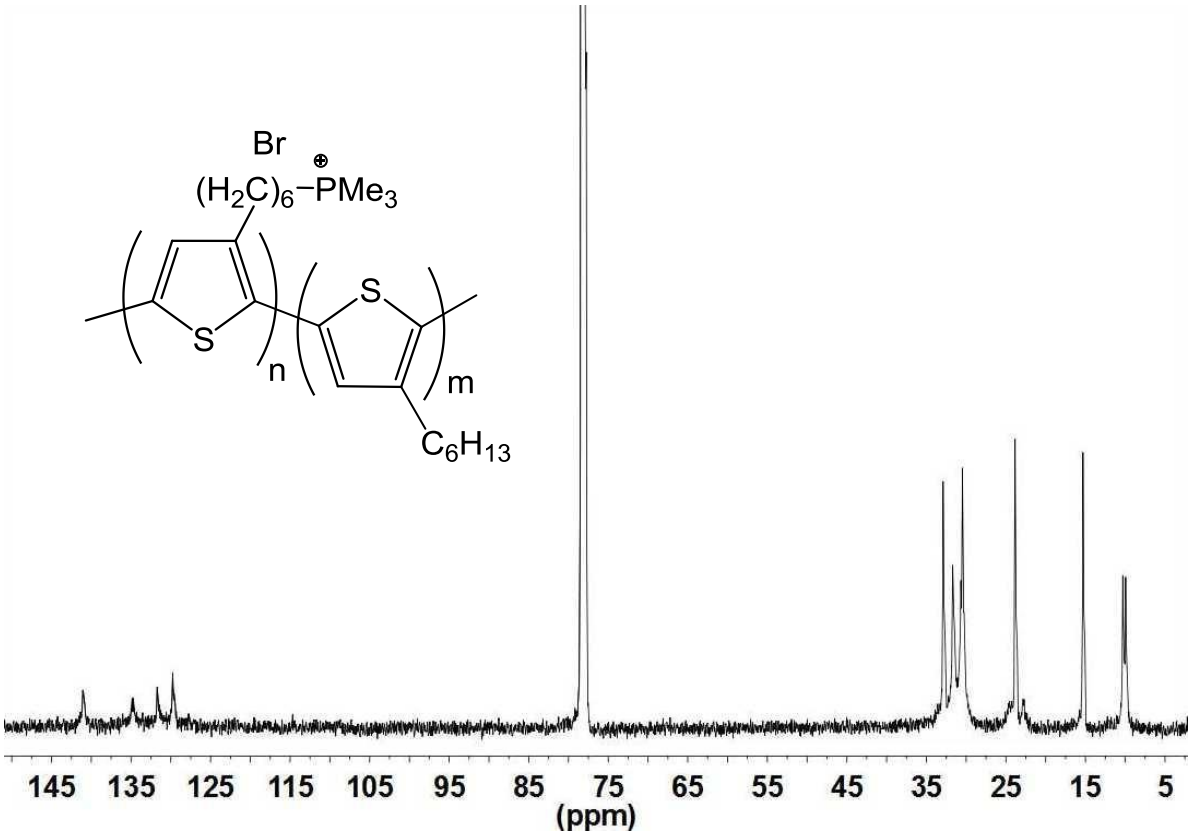

Figure S11. $^{13}C\{^{1}H\}$ NMR spectrum of **P3HT-*b*-P3HTPMe$_3$** in $CDCl_3$

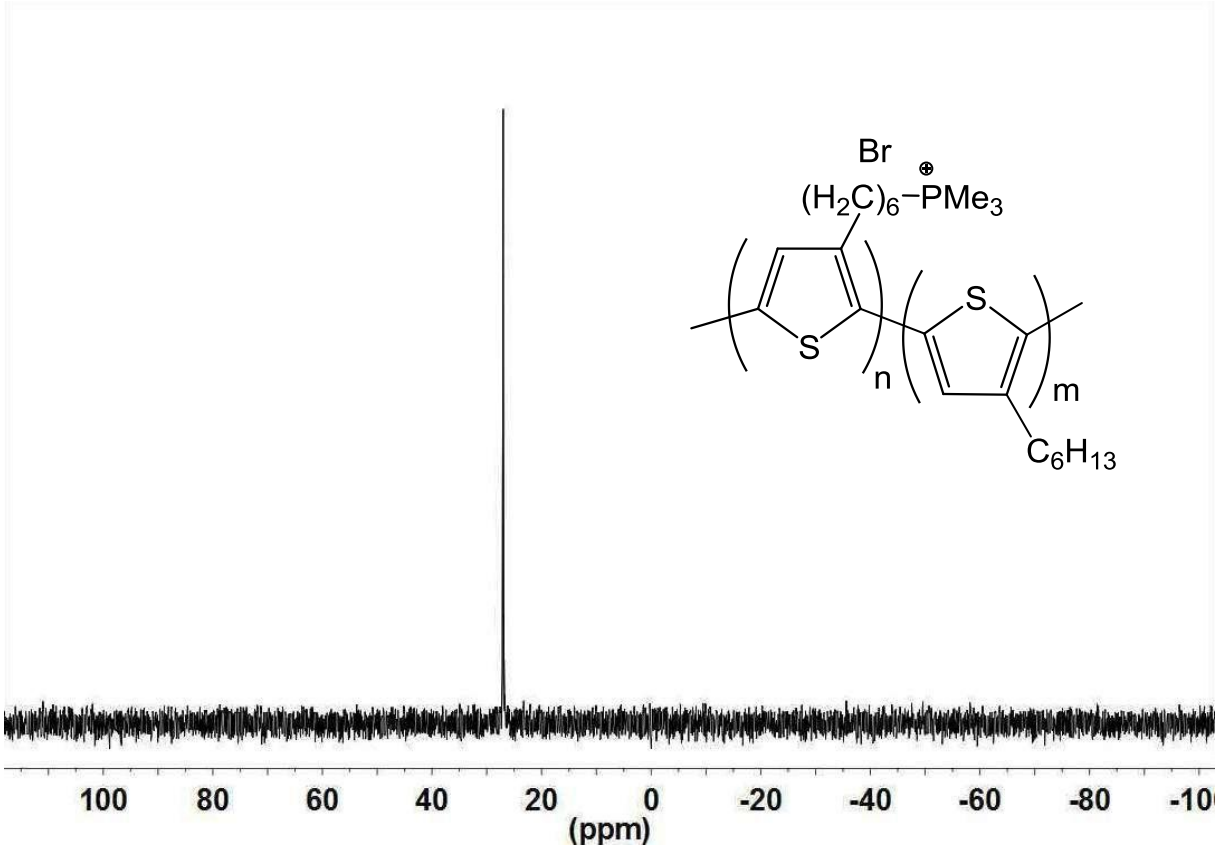

Figure S12. $^{31}P\{^{1}H\}$ NMR spectrum of **P3HT-*b*-P3HTPMe$_3$** in $CDCl_3$

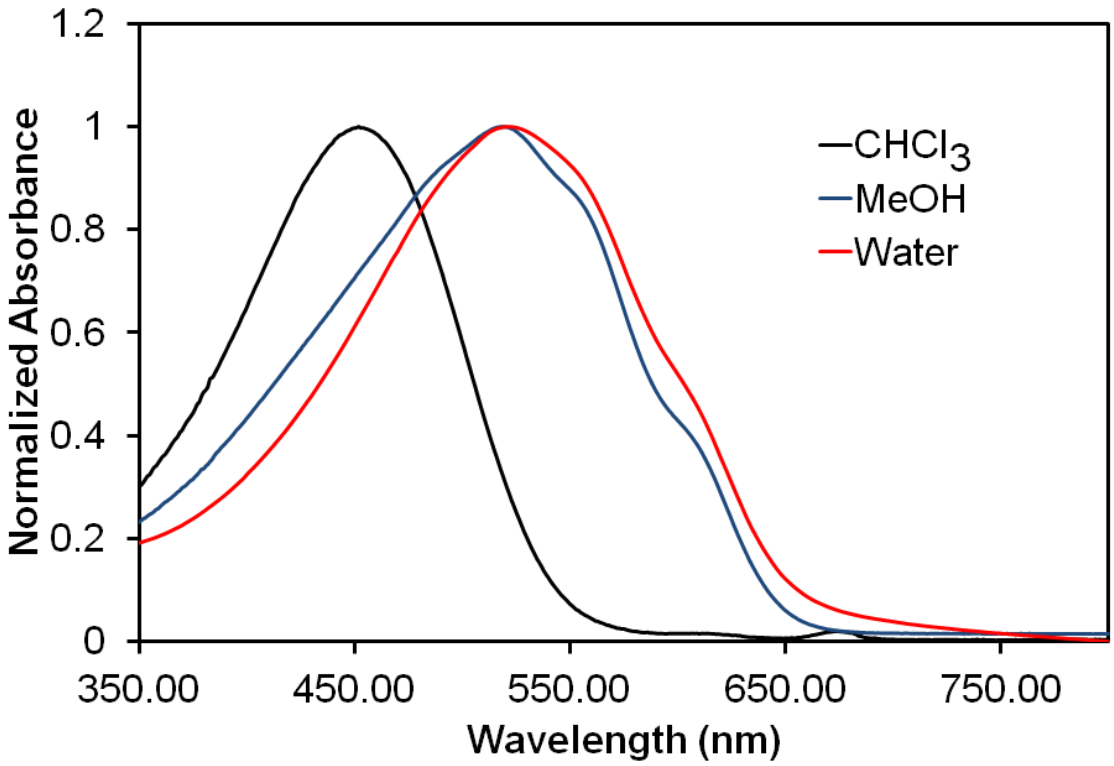

Figure S13. UV/Vis. absorption spectra of **P3HT-*b*-P3HTIm** in $CHCl_3$ (black), MeOH (blue) and water (red).

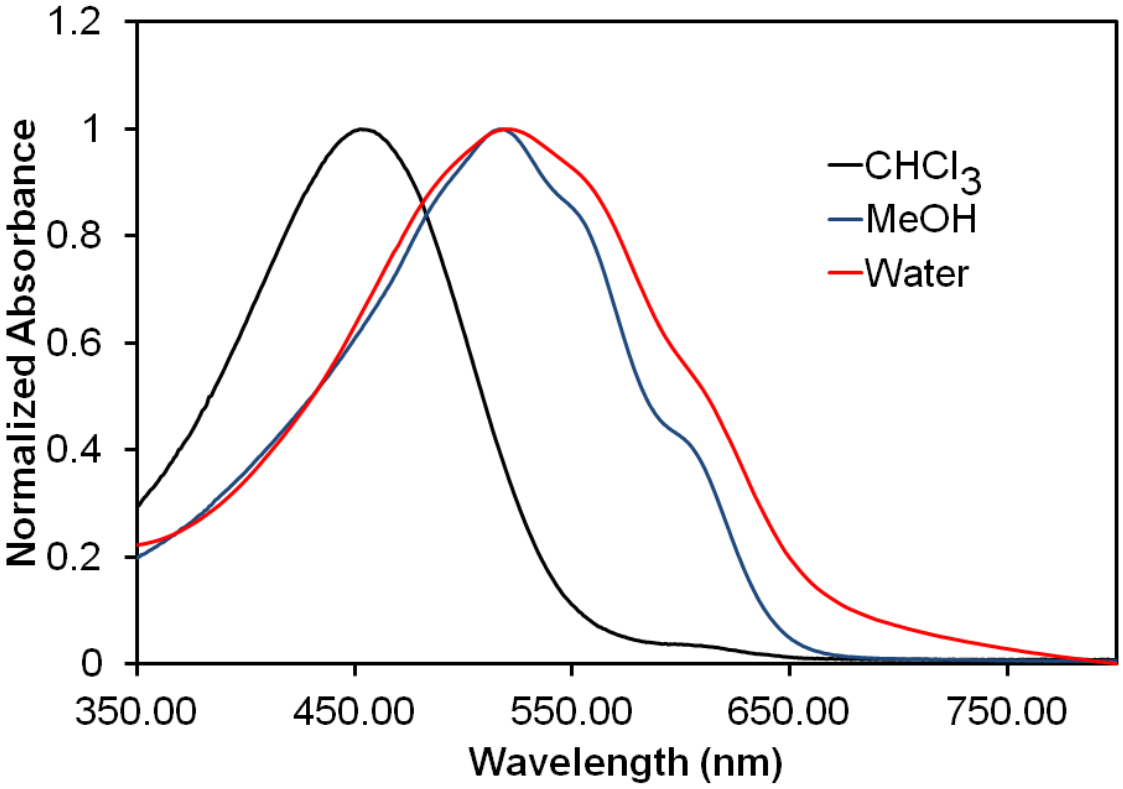

Figure S14. UV/Vis. absorption spectra of **P3HT-*b*-P3HTPy** in $CHCl_3$ (black), MeOH (blue) and water (red).

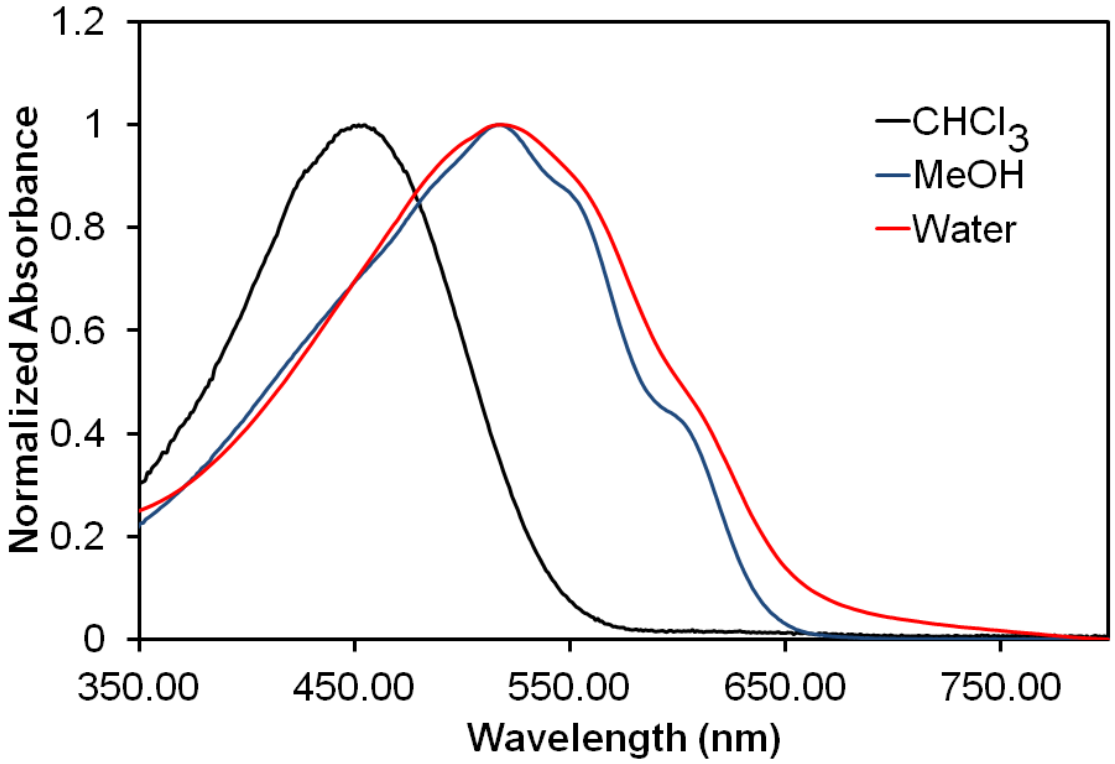

Figure S15. UV/Vis. absorption spectra of **P3HT-*b*-P3HTNMe$_3$** in $CHCl_3$ (black), MeOH (blue) and water (red).

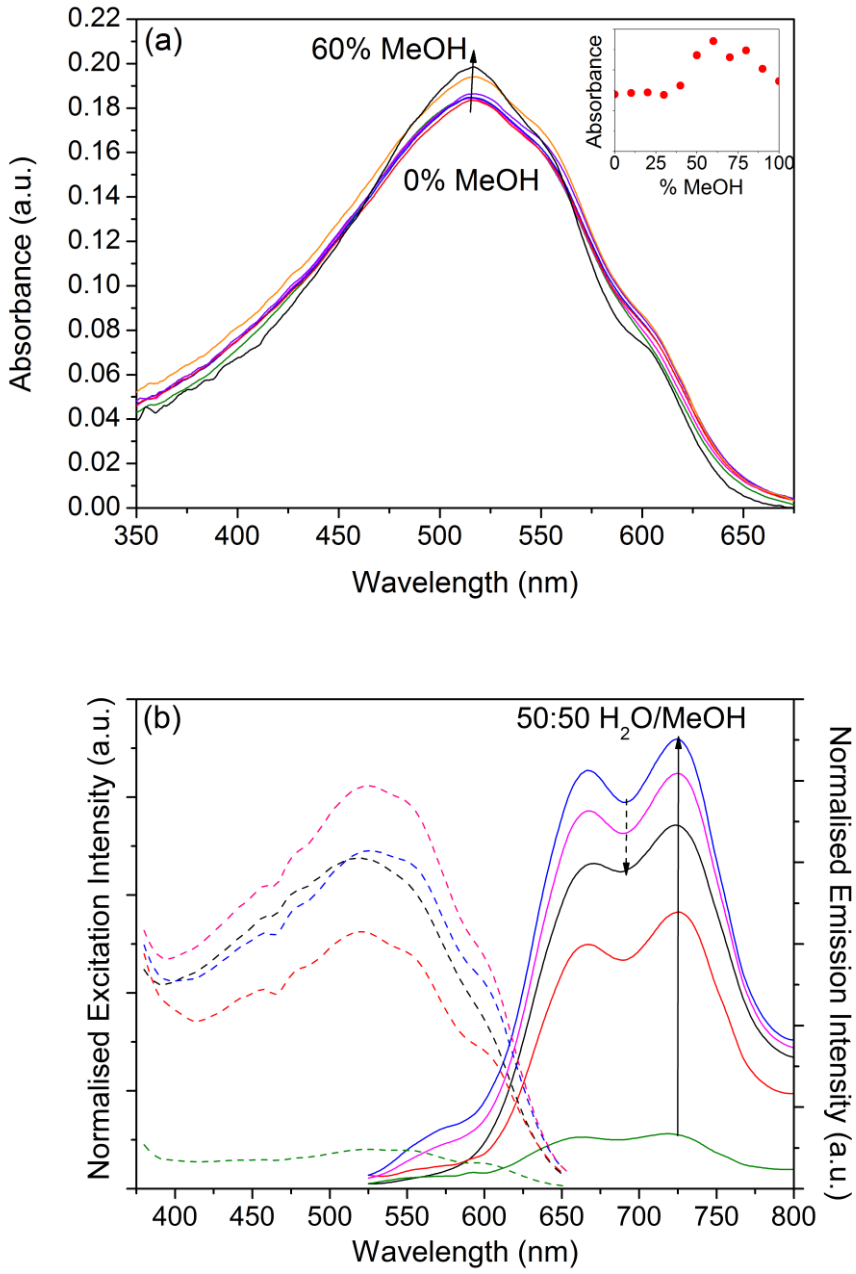

Figure S16. (a) UV/Vis absorption spectra of **P3HT-*b*-P3HTNMe$_3$** in 0-60% MeOH. Inset: Absorbance at λ_{max} = 514 nm as a function of vol% MeOH in H_2O/MeOH mixtures. (b) Selected excitation (λ_{em} = 723 nm) and PL (λ_{ex} = 514 nm) spectra of **P3HT-*b*-P3HTNMe$_3$** in 100% methanol (green line), 70% MeOH (red line), 50% MeOH (blue line), 40% MeOH (pink line) and 100% water (black line).

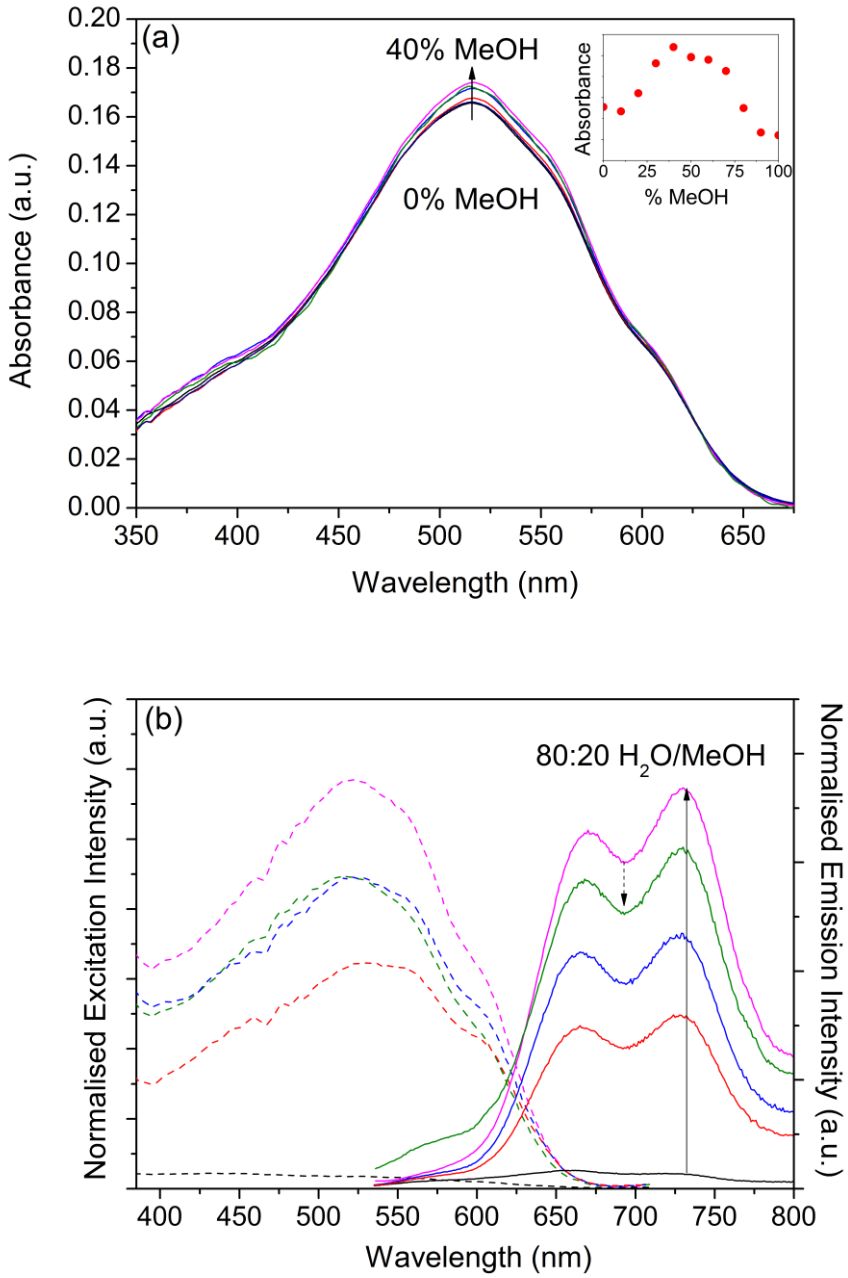

Figure S17. (a) UV/Vis absorption spectra of **P3HT-*b*-P3HTIm** in 0-40% MeOH. Inset: Absorbance at λ_{max} =515 nm as a function of vol% MeOH in H_2O/MeOH mixtures. (b) Selected excitation (λ_{em} = 730 nm) and PL (λ_{ex} = 515 nm) spectra of **P3HT-*b*-P3HTIm** in 100% methanol (black line), 60% MeOH (red line), 50% MeOH (blue line), 20% MeOH (pink line) and 0% MeOH (green line).

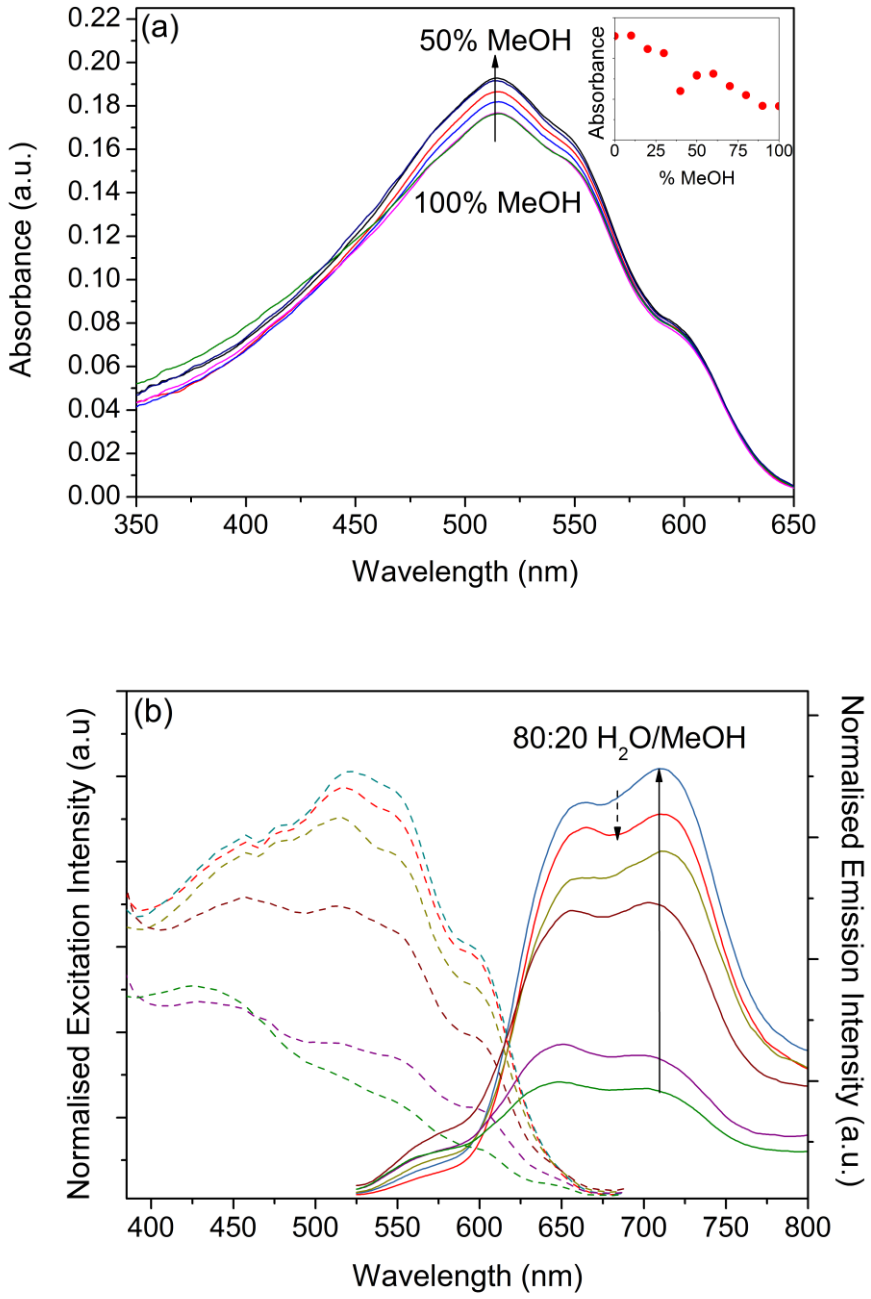

Figure S18. (a) UV/Vis absorption spectra of **P3HT-*b*-P3HTPMe$_3$** in 50-100% MeOH. Inset: Absorbance at λ_{max} = 514 nm as a function of vol% MeOH in H_2O/MeOH mixtures. (b) Selected excitation (λ_{em} = 730 nm) and PL (λ_{ex} = 514 nm) spectra of **P3HT-*b*-P3HTPMe$_3$** in 100% MeOH (green line), 80% MeOH (purple line), 60% MeOH (brown line), 40% MeOH (yellow line), 20% MeOH (blue line) and 0% MeOH (red line).

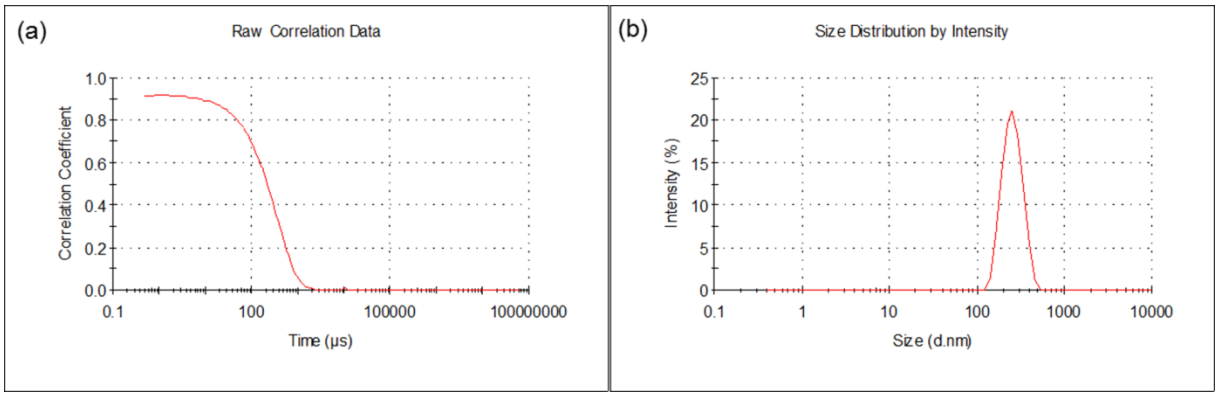

Figure S19. (a) A representative correlogram and (b) size distribution by intensity plot obtained by DLS of **P3HT-*b*-P3HTPMe$_3$** in MeOH (D_h of 244 nm and a PDI of 0.049).

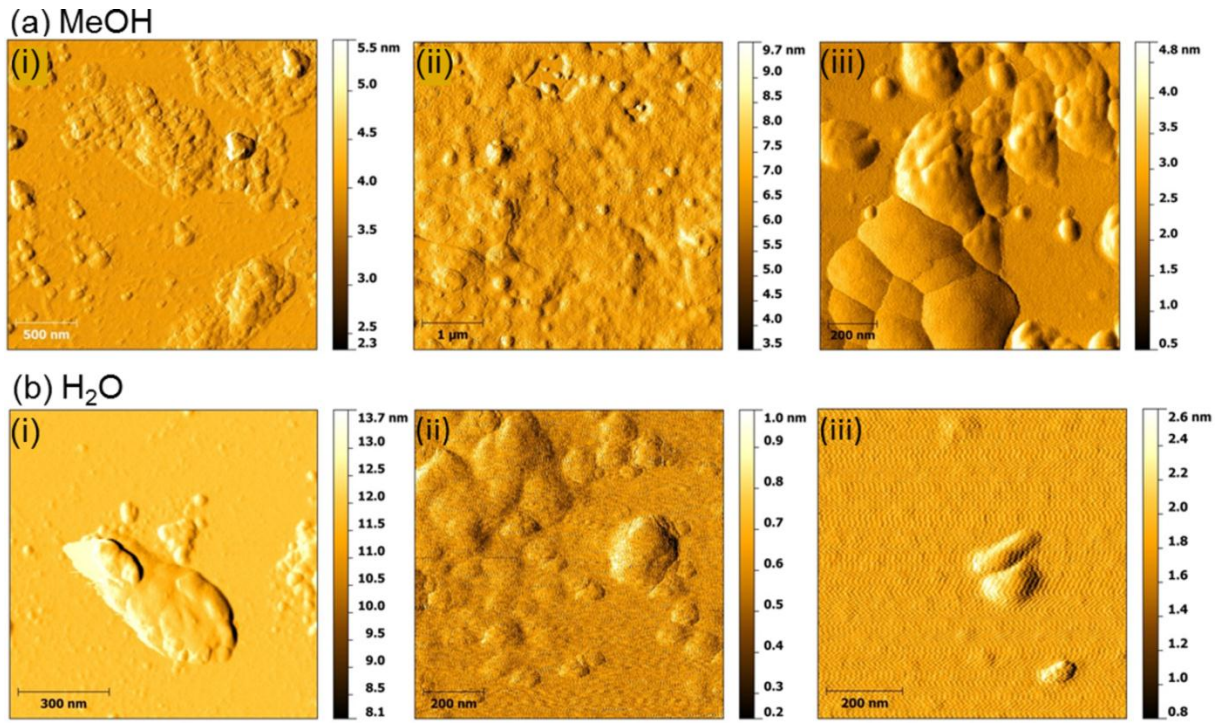

Figure S20. AFM amplitude images of **P3HT-*b*-CPEs** drop-cast onto freshly cleaved mica from (a) MeOH and (b) H_2O. (i) **P3HT-*b*-P3HTNMe$_3$** (3.5 µg mL^{-1}), (ii) **P3HT-*b*-P3HTPMe$_3$** (0.1 mg mL^{-1}) and (iii) **P3HT-*b*-P3HTPy** (3.5 µg mL^{-1}).

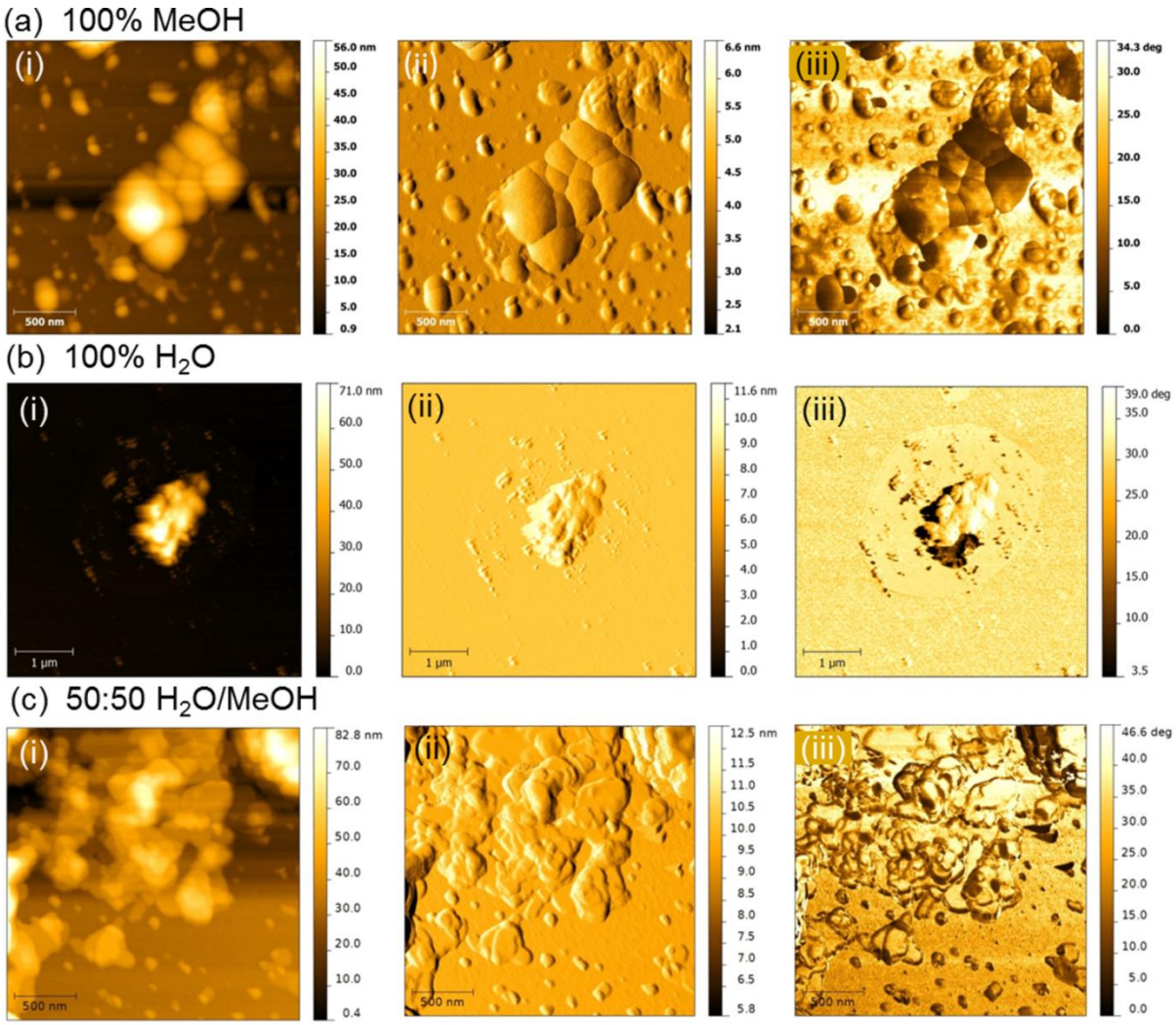

Figure S21. AFM images of **P3HT-*b*-P3HTPy** film drop-cast from (a) MeOH (3.5 µg mL^{-1}), (b) H_2O (3.5 µg mL^{-1}) and (c) 50:50 H_2O/MeOH (3.5 µg mL^{-1}) onto freshly cleaved mica. (i) Height, (ii) amplitude and (iii) phase images, respectively.

SANS and Core Shell Cylinder Model

The SANS scattering profiles were modelled using a Core Shell Cylinder model in the SasView programme using a non-linear least squares method.

The scattered SANS intensity is given by $I(q) = NV_s^2P(q)S(q) + bkg$, where N is the number of particles per unit volume, V_s is the total volume of the core plus shell, P is the form or shape factor, S is the structure factor and bkg is the background level. The form or shape factor, $P(q, \alpha)$, for the Core Shell Cylinder model is given by:

$$\varphi VsP(q,\alpha) = \frac{scale}{V_s}\int_0^{\pi/2} f^2\,(q)\,d\alpha \qquad (1)$$

where

$$f(q) = \frac{2(\rho_c-\rho_s)V_c \sin\left[qLcos(\frac{\alpha}{2})\right]}{\left[qLcos\left(\frac{\alpha}{2}\right)\right]\frac{J_1[qrsin\alpha]}{[qrsin\alpha]}} + \frac{2(\rho_s-\rho_{solv})V_s \sin\left[q(L+t)cos(\frac{\alpha}{2})\right]}{\left[q(L+t)cos\left(\frac{\alpha}{2}\right)\right]\frac{J_1[q(r+t)sin\alpha]}{[q(r+t)sin\alpha]}} \qquad (2)$$

where α is the angle between the axis of the cylinder and the q-vector, V_s is the total volume of the core plus shell, V_c is the volume of the core, L is the length of the core, r is the radius of the core, t is the thickness of the shell, ρ_c, ρ_s and ρ_{solv} are the scattering length densities of the core, shell and solvent, respectively, and bkg is the background level.[1] J_1 is the first order Bessel function. This model provides the form factor for a circular cylinder with a core-shell scattering length density profile. The form factor is normalised by the particle volume so that the scale factor of the fit is the total particle volume fraction $\varphi = NV_s$ when $I(q)$ has been correctly reduced to absolute units. The interparticle structure factor, $S(q)$, which accounts for the interference of scattering from different particles in concentrated suspensions, is assumed to be one. The concentration of the samples is notionally low (10 mg mL^{-1}), though the solvent included in the aggregates makes the effective volume fraction much higher, their relatively large size pushes any $S(q)$ to very low q. Attractive interactions would make $S(q)$ pull up the scattering at smallest q, in the

[1] I. Livesey, *J. Chem. Soc. Faraday Trans.* 2, 1987, **83**, 1445.

same manner as for any larger aggregates that may form The fitting procedure included polydispersity in the length and the radius of the rods and instrumental q smearing was applied to provide better fits at the high q end of the SANS data.

Core Shell Sphere Model

For the samples which were found to form "short-rods" with the Core-Shell-Cylinder Model, the SANS scattering profiles were also modelled using the Core-Shell-Sphere model in the SasView programme using a non-linear least squares method. The form factor, $P(q, \alpha)$, for the Core-Shell-Sphere model is given by:

$$\varphi VsP(q) = \frac{scale}{V_s} f^2(q) \qquad (3)$$

where

$$f(q) = 3V_c(\rho_c - \rho_s)\frac{[\sin(qr_c) - qr_c\cos(qr_c)]}{(qr_c)^3} + 3V_S(\rho_c - \rho_{solv})\frac{[\sin(qr_s) - qr_c\cos(qr_s)]}{(qr_s)^3} \qquad (4)$$

where V_s is the total volume of the outer shell, V_c is the volume of the core, r_c is the radius of the core, $r_s = r_c + t$ where t is the thickness of the shell, ρ_c, ρ_s and ρ_{solv} are the scattering length densities of the core, shell and solvent, respectively and *bkg* is the background level.[2] This model provides the form factor for a sphere with a core-shell scattering length density profile. The form factor is normalised by the particle volume. The interparticle structure factor, $S(q)$, is assumed to be one as discussed above. The fitting procedure included polydispersity in the radius of the spheres and instrumental q smearing was applied to provide better fits at the high q end of the SANS data.

[2] *Small Angle Scattering of X-rays*, A. Guinier and G. Fournet, John Wiley and Sons, 1955.

Aggregation numbers

To calculate the number of block copolymers in an average particle we used the following:

$$N_{agg} = \frac{V_{dry-core} + V_{dry-shell}}{V_{molar}} x\, N_A \quad (5)$$

where N_{agg} is the aggregation number, $V_{dry\text{-}core}$ is the volume of the dry core, $V_{dry\text{-}shell}$ is the volume of the dry shell, V_{molar} is the molar volume and N_A is the Avagadro's number.

Table S1. Structural parameters obtained SANS data for **P3HT-*b*-P3HTPy** and **P3HT-*b*-P3HTIm** in d_4-MeOD, D_2O and d_4-MeOD/D_2O mixtures: SLD_{sol} is the scattering length density of the solvent and α is the scattering power of the defined q region. L_{core}, r_{core} and T_{shell} are the core length, core radius and shell thickness, respectively, obtained from the best fits to the data using the Core-Shell-Cylinder Model in SasView. $X_{sol\text{-}core}$ and $X_{sol\text{-}shell}$ are the calculated solvent fractions in the core and shell, respectively.

CPE	Solvent	SLD_{sol} ($Å^{-2}$)	$q^{-\alpha}$ (q<0.2)	$q^{-\alpha}$ (0.2<q<0.7)	$q^{-\alpha}$ (q>0.7)	L_{core} (nm)	r_{core} (nm)	T_{shell} (nm)	$X_{sol\text{-}core}$	$X_{sol\text{-}shell}$
P3HT-*b*-P3HTPy	d_4-MeOD	5.8×10^{-6}	-1.5	-4.2	-1.83	80	6	2.0	0.81	0.65
P3HT-*b*-P3HTPy	50:50 (v/v) d_4-MeOD/D_2O	6.09×10^{-6}	-1.38	-4.76	-1.78	11	7.5	9.5	0.31	0.87
P3HT-*b*-P3HTPy	D_2O	6.38×10^{-6}	-5/3	-5.21	-1.54	9	5.5	8	0.65	0.89
P3HT-*b*-P3HTIm	d_4-MeOD	5.8×10^{-6}	-0.93	-4.29	-1.79	93	5.4	2	0.79	0.62
P3HT-*b*-P3HTIm	20:80 (v/v) d_4-MeOD/D_2O	6.26×10^{-6}	-1.36	-4.47	-1.73	12	9	11	0.45	0.96
P3HT-*b*-P3HTIm	D_2O	6.38×10^{-6}	-1.72	-5.05	-1.63	23	13	11	0.69	0.97

Table S2. Structural parameters obtained SANS data for **P3HT-*b*-P3HTPy** and **P3HT-*b*-P3HTIm** in D_2O and d_4-MeOD/D_2O mixtures: SLD_{sol} is the scattering length density of the solvent. r_{core} and T_{shell} are the core radius and shell thickness, respectively, obtained from the best fits to the data using the Core-Shell-Sphere Model in SasView. $X_{sol\text{-}core}$ and $X_{sol\text{-}shell}$ are the calculated solvent fractions in the core and shell, respectively. The aggregation numbers: $N_{agg\text{-}cylinder}$ and $N_{agg\text{-}sphere,}$ have been calculated for the Core-Shell-Cylinder Model and Core-Shell-Sphere Model fits.

CPE	Solvent	SLD_{sol} ($Å^{-2}$)	r_{core} (nm)	T_{shell} (nm)	$X_{sol\text{-}core}$	$X_{sol\text{-}shell}$	$N_{agg\text{-}cylinder}$	$N_{agg\text{-}sphere}$
P3HT-*b*-P3HTPy	d_4-MeOD	5.8×10^{-6}	-	-	-	-	166	-
P3HT-*b*-P3HTPy	50:50 (v/v) d_4-MeOD/D_2O	6.09×10^{-6}	74	106	0.67	0.94	197	84
P3HT-*b*-P3HTPy	D_2O	6.38×10^{-6}	59	95	0.54	0.86	88	101
P3HT-*b*-P3HTIm	d_4-MeOD	5.8×10^{-6}	-	-	-	-	209	-
P3HT-*b*-P3HTIm	20:80 (v/v) d_4-MeOD/D_2O	6.26×10^{-6}	77	115	0.39	0.94	151	124
P3HT-*b*-P3HTIm	D_2O	6.38×10^{-6}	79	122	0.42	0.86	244	236

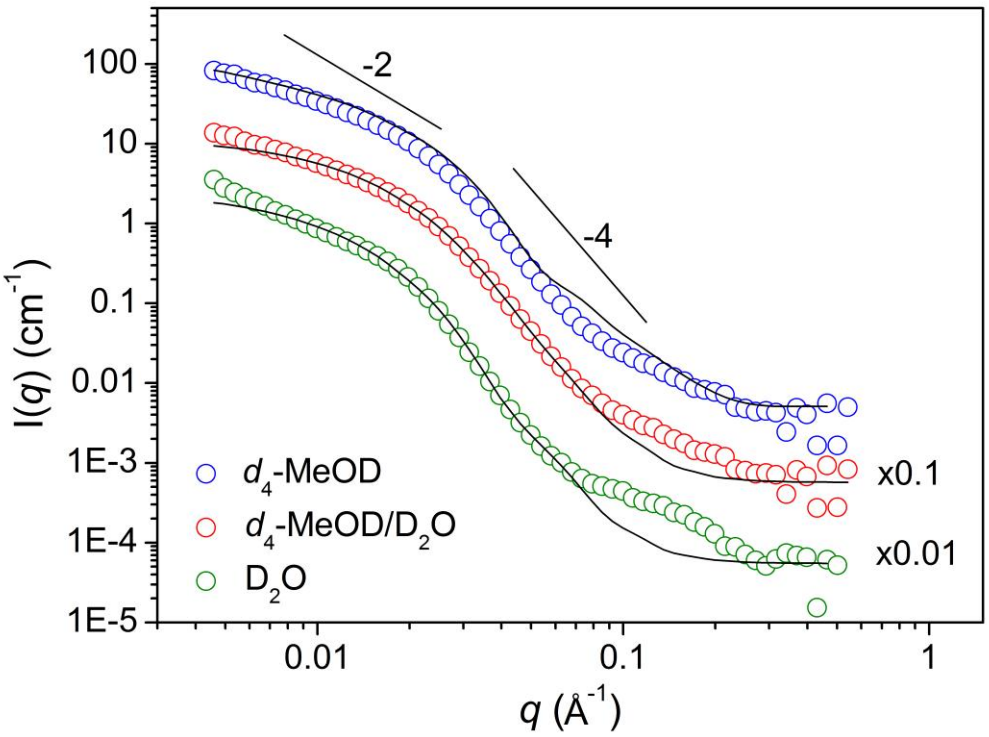

Figure S22. SANS data for **P3HT-*b*-P3HTIm** in, d_4-MeOD, 20:80 (v/v) d_4-MeOD/D_2O and D_2O. For clarity, the d_4-MeOD/D_2O and D_2O data have been multiplied by 0.1 and 0.01, respectively. Curved lines show the best fits of the scattering profiles using the Core-Shell Cylinder Model. For comparison, the straight solid lines show -2 decay for a Guassian coil and -4 decay for Porod decay.

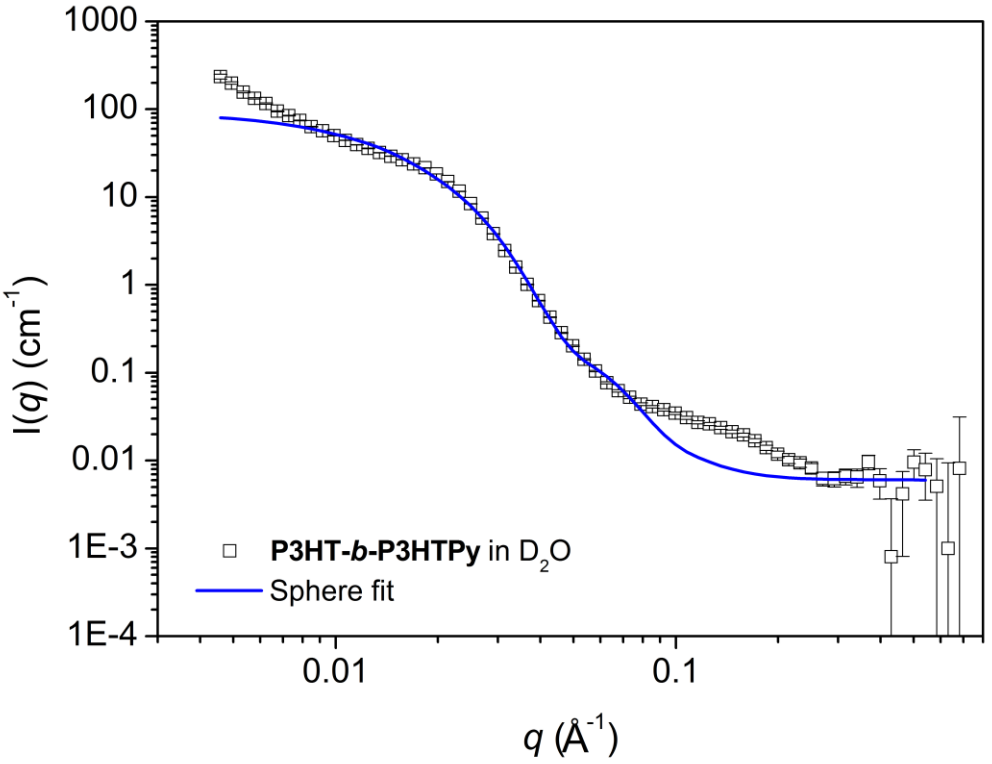

Figure S23. SANS data of **P3HT-*b*-P3HTPy** in D_2O modelled as spheres using the Core-Shell-Sphere model.

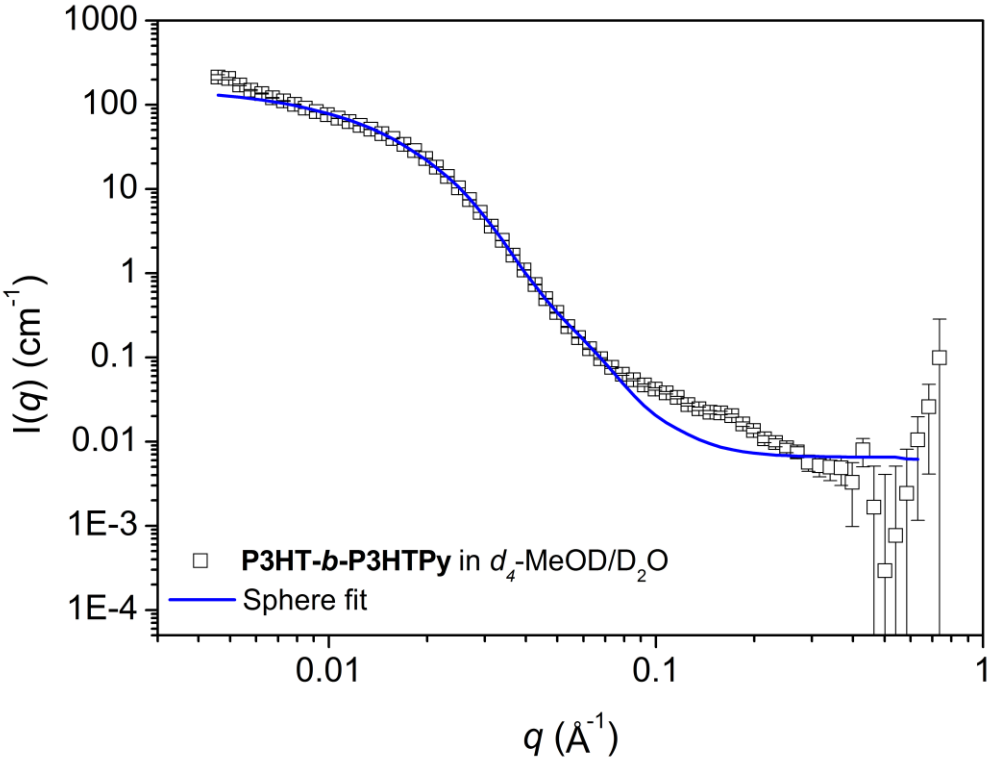

Figure S24. SANS data of **P3HT-*b*-P3HTPy** in 50:50 (v/v) D_2O/d_4-MeOD modelled as spheres using the Core-Shell-Sphere model.

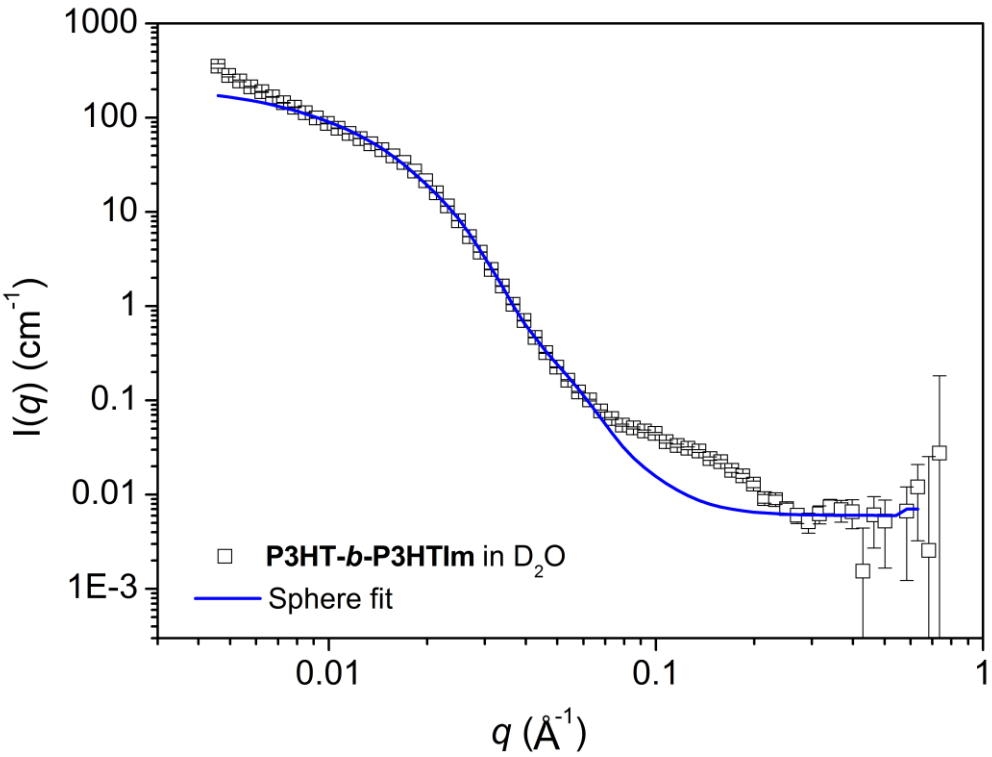

Figure S25. SANS data of **P3HT-*b*-P3HTIm** in D_2O modelled as spheres using the Core-Shell-Sphere model.

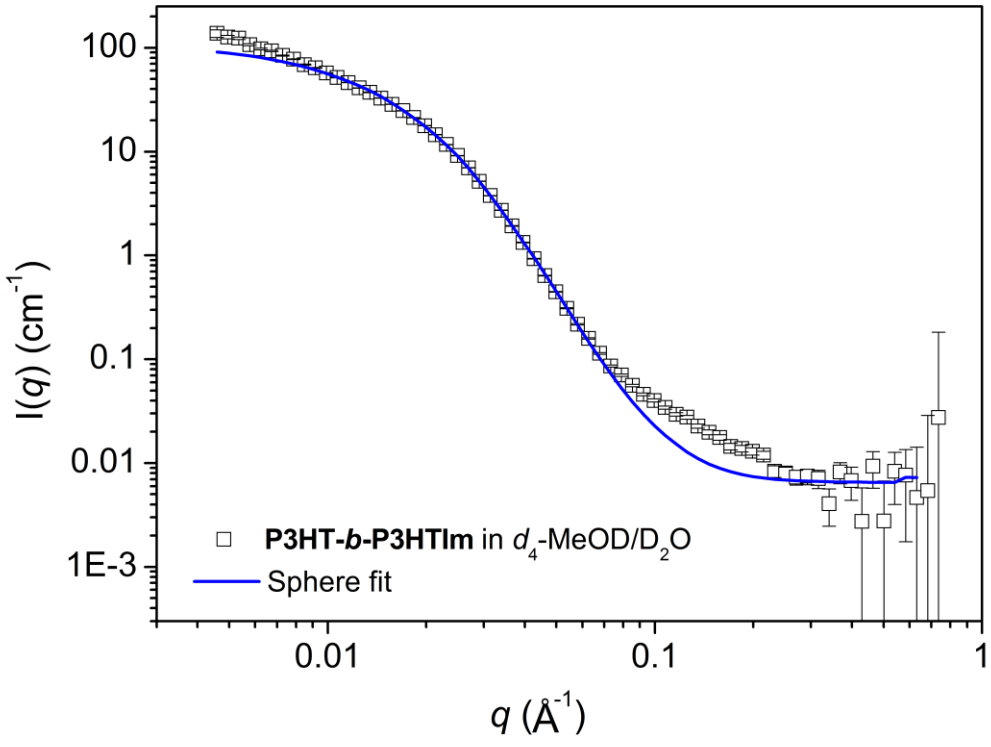

Figure S26. SANS data of **P3HT-*b*-P3HTIm** in 80:20 (v/v) D_2O/d_4-MeOD modelled as spheres using the Core-Shell-Sphere model.